

Cubosomes for *in vivo* fluorescence lifetime imaging

This content has been downloaded from IOPscience. Please scroll down to see the full text.

2017 Nanotechnology 28 055102

(<http://iopscience.iop.org/0957-4484/28/5/055102>)

View [the table of contents for this issue](#), or go to the [journal homepage](#) for more

Download details:

IP Address: 132.68.141.97

This content was downloaded on 29/05/2017 at 10:23

Please note that [terms and conditions apply](#).

You may also be interested in:

[Targeted lipid-polyaniline hybrid nanoparticles for photoacoustic imaging guided photothermal therapy of cancer](#)

Jinping Wang, Ran Yan, Fang Guo et al.

[A multi-functional nanoplatform for tumor synergistic phototherapy](#)

Huijuan Zhang, Xiaojing Jiao, Qianqian Chen et al.

[Serum-stable quantum dot--protein hybrid nanocapsules for optical bio-imaging](#)

Jeong Yu Lee, Dong Heon Nam, Mi Hwa Oh et al.

[Poly\(D, L-lactide-co-glycolide\) nanoparticles as delivery agents for photodynamic therapy: enhancing singlet oxygen release and phototoxicity by surface PEG coating](#)

Ester Boix-Garriga, Pilar Acedo, Ana Casadó et al.

[Lactobionic acid-conjugated TPGS nanoparticles for enhancing therapeutic efficacy of etoposide against hepatocellular carcinoma](#)

Altansukh Tsend-Ayush, Xiumei Zhu, Yu Ding et al.

[Encapsulation of palladium porphyrin photosensitizer in layered metal oxide nanoparticles for photodynamic therapy against skin melanoma](#)

Zih-An Chen, Yaswanth Kuthati, Ranjith Kumar Kankala et al.

[Cathepsin B-degradable, NIR-responsive nanoparticulate platform for target-specific cancer therapy](#)

Sam P Tarassoli, Alejandra Martinez de Pinillos Bayona, Hayley Pye et al.

[Diagnosing gastrointestinal stromal tumours by single photon emission computed tomography using nano-radiopharmaceuticals based on bevacizumab monoclonal antibody](#)

Thais Braga Ligiero, Cristal Cerqueira-Coutinho, Marta de Souza Albernaz et al.

Cubosomes for *in vivo* fluorescence lifetime imaging

Stefania Biffi^{1,10}, Laura Andolfi², Claudia Caltagirone³, Chiara Garrovo¹, Angela M Falchi⁴, Vito Lippolis³, Andrea Lorenzon⁵, Paolo Macor⁶, Valeria Meli³, Maura Monduzzi³, Marc Obiols-Rabasa⁷, Luca Petrizza⁸, Luca Prodi⁸, Antonella Rosa⁴, Judith Schmidt⁹, Yeshayahu Talmon⁹ and Sergio Murgia^{3,10}

¹Institute for Maternal and Child Health—IRCCS ‘Burlo Garofolo’, Trieste, Italy

²IOM-CNR, Area Science Park, Basovizza, Trieste, Italy

³Department of Chemical and Geological Science, University of Cagliari, and CSGI, I-09042 Monserrato (CA), Italy

⁴Department of Biomedical Science, University of Cagliari, I-09042 Monserrato (CA), Italy

⁵Animal Care Unit, Cluster in Biomedicine (CBM srl), Trieste, Italy

⁶Department of Life Sciences, University of Trieste, Italy

⁷Division of Physical Chemistry, Department of Chemistry, Lund University Getingevägen 60, SE-22240 Lund, Sweden

⁸Department of Chemistry ‘G. Ciamician’, University of Bologna, Bologna, Italy

⁹Department of Chemical Engineering, Technion—Israel Institute of Technology, Haifa 3200003, Israel

E-mail: stefania.biffi@burlo.trieste.it and murgias@unica.it

Received 22 September 2016, revised 21 November 2016

Accepted for publication 30 November 2016


Published 29 December 2016



CrossMark

Abstract

Herein we provided the first proof of principle for *in vivo* fluorescence optical imaging application using monoolein-based cubosomes in a healthy mouse animal model. This formulation, administered at a non-cytotoxic concentration, was capable of providing both exogenous contrast for NIR fluorescence imaging with very high efficiency and chemospecific information upon lifetime analysis. Time-resolved measurements of fluorescence after the intravenous injection of cubosomes revealed that the dye rapidly accumulated mainly in the liver, while lifetimes profiles obtained *in vivo* allowed for discriminating between free dye or dye embedded within the cubosome nanostructure after injection.

 Online supplementary data available from stacks.iop.org/NANO/28/055102/mmedia

Keywords: liquid crystalline nanoparticles, fluorescence lifetime probe, fluorescence optical imaging *in vivo*

(Some figures may appear in colour only in the online journal)

1. Introduction

Spontaneous self-assembly of lipids in water permits the formulation of liquid crystalline nanoparticles of the inverted type, showing inner nanostructure characterized by lipid bilayers wrapped on triply periodic minimal surfaces of cubic symmetry [1–4], a beautiful three-dimensional organization now completely disclosed by cryo-electron tomography [5].

Discovered in the eighties, such nanoparticles are universally known as cubosomes [6, 7]. They are considered an emerging platform for a wide range of nanomedicine applications by virtue of unique features [8]. These include a high hydrophobic volume (higher than liposomes) [9], the possibility of simultaneously hosting both diagnostic agents and therapeutics (cubosomes are also proposed as theranostic tools) [9–11], storage stability, and a viscosity similar to water, which is a fundamental characteristic for bolus delivery [12]. Recently, they were successfully tested as carriers for

¹⁰ Author to whom all correspondence should be addressed.

antimicrobial peptides [13], and their superior efficacy in the siRNA delivery (cuboplexes) with respect to traditional lipoplexes was also demonstrated [14]. The necessary colloidal stability of cubosome formulations is typically achieved by using polyethylene oxide (PEO)-polypropylene oxide (PPO)-polyethylene oxide triblock copolymers (Pluronics) as stabilizing agents, although other kinds of stabilizers have been proposed [14–18]. As a consequence, cubosomes are surrounded by a PEO corona that, similarly to stealth liposomes, should retard clearance of these nanoparticles from the bloodstream via the mononuclear phagocytic system by inhibiting opsonization [19, 20]. Furthermore, their surface can be decorated with targeting residues to properly address cubosomes toward specific tissues [21, 22]. Despite their remarkable potential as nanocarriers, to the best of our knowledge, so far, no papers have appeared describing the successful exploitation of cubosomes for *in vivo* imaging. Several authors have demonstrated that the hexagonal counterpart of cubosomes (namely, hexosomes) can be effectively labeled with radiotracers (such as ^{99}Tc) [23, 24] or MRI contrast agents (paramagnetic nitroxide lipids) [12, 25], providing valuable imaging tools for *in vivo* diagnostics. Compared with traditional structural and functional imaging modalities, fluorescence optical imaging (FOI) offers several advantages, requiring a relatively simple instrumental setup, and showing high signal-to-noise ratios *in vivo*, owing to the development of novel synthetic fluorescent probes with high brightness and photostability in the near infrared spectral region (NIR, 650–900 nm) [26–29]. Therefore, innovative FOI methods hold promise as radiation-free, portable, and potentially cost-effective screening technology extremely useful in imaging studies *in vivo* [30]. In particular, time-domain optical imaging (TD-OI) technology allows for NIR fluorescence lifetime analysis, which is based both on the specificity of fluorescence probes and the sensitivity of their emission lifetime, related to environmental characteristics [31–36]. In this context, here we provide the first proof of principle for FOI application using monoolein (MO)-based cubosomes *in vivo* in a healthy mouse animal model.

2. Materials and methods

2.1. Cubosomes preparation and characterization

Cubosomes were prepared by dispersing melted MO (1-monooleoylglycerol, 98.1 wt%, Danisco A/S, DK-7200, Grinsted, Denmark) in an aqueous solution of Pluronic F108 (PF108, PEO₁₃₂-PPO₅₀-PEO₁₃₂, Sigma-Aldrich) using an ultrasonic processor UP100H, provided by Dr Hielscher, with a 0.9 cycle and 90% amplitude for 10 min. To obtain fluorescent cubosomes, the fluorophore Cy5.5-C₁₄ was dispersed in the melted MO with the help of an ultrasonic bath before dispersion in Pluronic F108. Typical sample volume sample was 4 ml with 96.4 wt% of water, 3.3 wt% of MO, and 0.3 wt% of Pluronic F108. After loading, cubosome dispersion was purified from the non-encapsulated dye by dialysis as follows: 2 ml were loaded into a dialysis tubing cellulose

membrane (14 kDa MW cutoff, Sigma-Aldrich) and dialyzed against water (1000 ml) for 2 h (by replacing the water after 1 h). Loading efficiency ($E\%$), expressed as percentage of the amount of the dye present in the formulation before dialysis, was determined by UV-vis spectroscopy after disruption of cubosomes (dialyzed and not dialyzed) with acetonitrile. Cy5.5-C₁₄ content was quantified before and after purification by a Thermo Nicolet Evolution 300 UV-vis spectrophotometer at 679 nm. The molar concentration of Cy5.5-C₁₄ in the cubosomes sample after dialysis was 2.7×10^{-4} , with $E\% = 75$. Dynamic light scattering (DLS) measurements for the determination of nanoparticle size and ζ -potential were performed at 25 °C using a ZetaSizer Nano ZSP (Malvern Instruments Ltd, Worcestershire, UK). To confirm that injection did not alter the physicochemical characteristics of the formulation, DLS measurements were also performed after the cubosome formulation was passed through a 30 G needle (the same used for cubosome intravenous (i.v.) administration for *in vivo* tests). Characterization of the nanoparticles' internal structure at 25 °C was conducted by small-angle x-ray scattering (SAXS) using a Ganesha 300XL (SAXSLAB ApS, Skovlunde, Denmark). The lattice parameter a of the cubic phases was determined using the relation $a = d(h^2 + k^2 + l^2)^{1/2}$ from linear fits of the plots of $1/d$ versus $(h^2 + k^2 + l^2)^{1/2}$, where $d = 2\pi/q$. q is the measured peak position, and h , k , and l are the Miller indices. The a value is the average (\pm SD) value calculated from the five Bragg peaks discernible in the diffractogram (see figure 1(b)). The morphology of the nanoparticles was observed at 120 kV acceleration voltage in an FEI Tecnai T12 G² transmission electron microscope at about -175 °C in the low-dose imaging mode to minimize electron beam radiation damage. Images were digitally recorded with a Gatan US1000 high-resolution charge coupled device (CCD) camera.

2.2. Photophysical measurements

Cubosome solutions were diluted with Milli-Q[®] water. UV-vis absorption spectra were recorded at 25 °C by means of a Perkin-Elmer Lambda 45 spectrophotometer. Quartz cuvettes with an optical path length of 1 cm were used. Corrected fluorescence emission and excitation spectra (450 W, Xe lamp) were obtained with a modular UV-vis-NIR spectrofluorometer (Edinburgh Instruments FLS920) equipped with both a Hamamatsu R928P photomultiplier tube (for the 500–850 nm spectral range) and an Edinburgh Instruments Ge detector (for the 800–1600 nm spectral range). Luminescence quantum yields (uncertainty $\pm 15\%$) were recorded on air-equilibrated solutions and cyanine IR-125 (Acros Organics) in ethanol ($\Phi = 0.132$) [37]. The same instrument connected to a PCS900 PC card was used for the time-correlated single photon counting (TCSPC) experiments (excitation laser $\lambda = 640$ nm). Corrections for instrumental response, inner filter effects, and phototube sensitivity were performed [38]. Fluorescence anisotropy measurements were performed on an Edinburgh FLS920 equipped with Glan-Thompson polarizers. Anisotropy measurements were collected using an L-format configuration, and data were corrected for

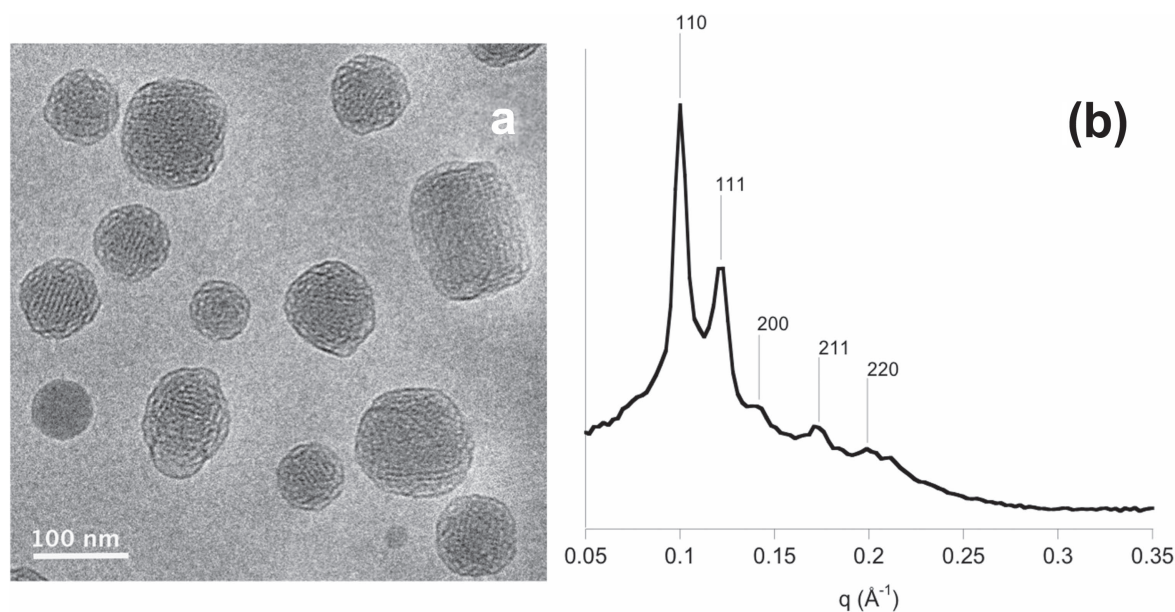


Figure 1. (a) Cryo-TEM image and (b) SAXS pattern at 25 °C of the cubosome formulation loaded with the Cy5.5- C₁₄ dye. Miller indices are shown on top of the corresponding Bragg peak.

polarization bias using the G-factor. Four different spectra were acquired for each sample combining different orientation of the excitation and emission polarizers: I_{VV} , I_{VH} , I_{HH} , I_{HV} (where V stands for vertical and H for horizontal; the first subscript refers to the excitation polarizer and the second subscript refers to the emission polarizer). Spectra were used to calculate the G-factor and anisotropy r : $G = I_{HV}/I_{HH}$, and $r = (I_{VV} - GI_{VH})/(I_{VV} + 2GI_{VH})$. The calculated G value was 1.85.

2.3. Cytotoxicity experiments

Mouse 3T3 fibroblasts (ATCC collection) were grown in phenol red-free Dulbecco's modified Eagle's medium (DMEM, Invitrogen, USA) with high glucose, supplemented with 10% (v/v) fetal bovine serum, penicillin (100 U ml⁻¹), and streptomycin (100 µg ml⁻¹) (Invitrogen) in a 5% CO₂ incubator at 37 °C. The cytotoxic effect of the nanoparticle formulation was evaluated in 3T3 fibroblasts by 3-(4,5-dimethylthiazolyl-2)-2, 5-diphenyltetrazolium bromide (MTT) assay [39]. 3T3 cells were seeded in 96-well plates at a density of 2×10^3 cells/well in 100 µl of serum-containing media. Experiments were conducted two days after seeding, when cells had reached 70% confluence. Cubosomes were added to the cells at different concentrations (corresponding to 20, 30, 40, 55, 83, and 165 µg ml⁻¹ of MO) in 100 µl of serum-free medium, and incubated at 37 °C for 4 h. The cell culture medium was then removed from each well of the 96-well plates; an 8 µl portion of MTT solution (3-(4,5-dimethylthiazol-2-yl)-2, 5-diphenyltetrazolium bromide) (5 mg ml⁻¹ in H₂O) was added to cells in fresh medium and left for 2 h at 37 °C. The medium was aspirated, 100 µl of Dimethyl sulfoxide (DMSO) was added to the wells, and color development was measured at 570 nm with an Infinite 200 auto microplate reader (Infinite 200, Tecan, Austria). The

absorbance is proportional to the number of viable cells. All measurements were performed in quadruplicate and repeated at least three times. Results are shown as the percent of cell viability in comparison with non-treated control cells. Evaluation of statistical significance of differences was performed using GraphPad INSTAT software (GraphPad software, San Diego, CA, USA). Comparison between groups was assessed by one-way analysis of variance (one-way ANOVA) followed by the Bonferroni multiple comparisons test.

2.4. Hemolytic assays

These assays were done as previously described [40]. Briefly, hemolytic activity was performed by mixing different amounts of cubosomes in veronal buffer with 50 µl of 10% human erythrocytes suspended in a final volume of 250 µl. After incubation at 37 °C for 30 min, red cell lysis was calculated by measuring the OD415. Hemolytic activity was expressed as a percentage of lysis ± SD.

2.5. Animal model and treatment

Pathogen-free female BALB/c mice (4 to 6 weeks old) were purchased from Harlan Laboratories (San Pietro al Natisone, Italy). Mice were housed in a controlled environment and maintained with *ad libitum* food and water. Mice were treated intravenously with 150 µl of cubosomes solution, corresponding to ~0.4 nmol Cy5.5-C₁₄ and 50 µg MO. Mice were followed by optical image acquisition over time to evaluate the probe biodistribution and accumulation in specific organs. Animals were also subjected to blood samples for plasma collection.

2.6. *In vivo* and *ex vivo* time-domain optical imaging analysis

Experimental animals were anesthetized with isoflurane at 1.8–2.0 volume %, shaved in the abdomen to avoid laser scattering caused by fur, placed in the small animal time-domain Optix MX2 preclinical NIRF-imager (Advanced Research Technologies, Montreal, CA), and maintained under vaporized isoflurane for the entire imaging session. Two-dimensional regions of interest were selected and laser power, integration time, and scan step size were optimized according to the emitted signal. A blank image was acquired before *i.v.* administration of cubosomes to record background signal intensity. After *i.v.* treatment the animals were monitored at multiple time points. In all imaging experiments, a 670 nm pulsed laser diode with a repetition frequency of 80 MHz and a time resolution of 12 ps light pulse was used for excitation. Fluorescence emission was collected at 700 nm and optical imaging results were analyzed by reporting fluorescence intensity values in normalized counts (NCs), representing the photon count for unit excitation laser power and unit exposure time, allowing comparison among different images. The fluorescence lifetime results were obtained by fitting every fluorescence decay curve corresponding to each pixel measured by the Optix system using the Levenberg Marquet least squares method [41]. For *ex vivo* imaging, the last *in vivo* whole body imaging session was followed by euthanasia of animals. Explanted organs were collected, washed in PBS, and analyzed with the same Optix system. Then, explanted organs were snap-frozen in isopentane and dry ice, and cooled at -80°C for tissue analysis.

2.7. *Ex vivo* tissue analysis

For fluorescence microscopy, sections of 7 and 12 μm thickness were cut from frozen organs with a cryostat at -20°C . Glass slides were kept at 4°C in the dark, and Vectashield Mounting Medium with 4',6-diamidino-2-phenylindole (DAPI) (Vector Laboratories, Burlingame, CA), diluted 1:1 with PBS, was used to stain cell nuclei. Fluorescent images were acquired by using an inverted microscope with a CCD camera (DVC-1412AM monochrome digital camera quantum efficiency $> 62\%$ at 550 nm) and 10X, 40X, and 63X objective lenses (NA 1.63) with immersion oil.

2.8. Ethical statement

All animal procedures were conducted to minimize animal pain and suffering. All experimental procedures were performed in strict accordance with the recommendations in the Guide for the Care and Use of Laboratory Animals of the National Institutes of Health and in compliance with European (86/609/EEC) and Italian (D.L.116/92) laws. Protocols for mice experimentation were approved by the Institutional Animal Care and Use Committee of the Cluster in Biomedicine (CBM) of the Area Science Park of Trieste and by the Italian Ministry of Health (DM 17/2001-A dd. 02/02/2011).

3. Results and discussion

To favor its encapsulation within the MO bilayer, a Cyanine 5.5 was modified by adding a long hydrocarbon chain (Cy5.5-C₁₄, see supplementary data for details). The fluorescent cubosome formulation was easily prepared by dispersing MO and Cy5.5-C₁₄ in a Pluronic F108 (PF108) aqueous solution. Physicochemical characterization of the formulation was performed by DLS, TEM at cryogenic temperature (cryo-TEM), and SAXS. According to DLS results, the formulation was a homogeneous dispersion (polydispersity index of 0.12) of nanoparticles characterized by a mean diameter of 144 ± 1 nm (see figure S1) and a ζ -potential of -21 mV. Nanoparticle morphology, as seen by cryo-TEM, revealed the co-existence of cubic-shaped and quasi-spherical objects both displaying an inner structure made of a dark matrix and alternate bright spots (figure 1(a)), as usually observed in bicontinuous cubic liquid crystalline nanoparticles (cubosomes). The nature of the liquid crystalline phase was assessed by SAXS. The diffraction pattern was characterized by at least five Bragg peaks with relative positions $\sqrt{2}:\sqrt{3}:2:\sqrt{6}:\sqrt{8}$ (figure 1(b)), confirming that the inner nanostructure was made of a bicontinuous cubic double diamond phase (space group *Pn3m*), having a lattice parameter of 89.1 ± 0.4 Å. Such a value is about 10% smaller than that recorded in pristine cubosomes (not containing the fluorescent probe) obtained using the same components [21]. This fact implicitly indicates that, although the nanostructure is retained, accommodation of Cy5.5-C₁₄ within the lipid bilayer alters the MO effective packing parameter [42], inducing a slightly higher curvature at the MO/water interface, and a consequential decrease in the lattice parameter.

Photophysical characterization of the dye and cubosome formulation was performed by UV-vis and fluorescence spectroscopy. As shown in figure S2 and reported in table S1, the free dye Cy5.5-C₁₄ showed, in EtOH, an absorption band centered at 685 nm ($\epsilon = 140\,000\text{ M}^{-1}\text{ cm}^{-1}$) with a shoulder at 650 nm ($\epsilon = 14\,000\text{ M}^{-1}\text{ cm}^{-1}$). A strong emission at 709 nm was observed ($\Phi = 0.27$). Once encapsulated inside the cubosomes (Cy5.5-C₁₄@cubosomes, aqueous dispersion), both the absorption ($\lambda_{\text{abs}} = 696$ nm and 665 nm) and emission bands ($\lambda_{\text{emis}} = 719$ nm) of the dye were slightly red-shifted (figure S3), probably due to the more apolar environment experienced by the fluorophore inside the nanoparticles with respect to EtOH. Moreover, a significant difference was recorded between the *r* value of the free dye and the encapsulated dye ($r = 0.008$ and $r = 0.100$ for Cy5.5-C₁₄ and Cy5.5-C₁₄@cubosomes, respectively). This difference is caused by the reduced mobility of the fluorophore inside the nanoparticles, and gives another proof of the internalization of Cy5.5-C₁₄ inside the cubosome formulation.

Before *in vivo* evaluation as a diagnostic tool, the formulation was tested *in vitro* for its toxicity. Indeed, several recent *in vitro* investigations drew attention to the potential cytotoxicity of cubosomes and, particularly, to their hemolytic properties [43, 44]. Remarkably, some evidence shows that stabilization of these kind of nanoparticles by means of

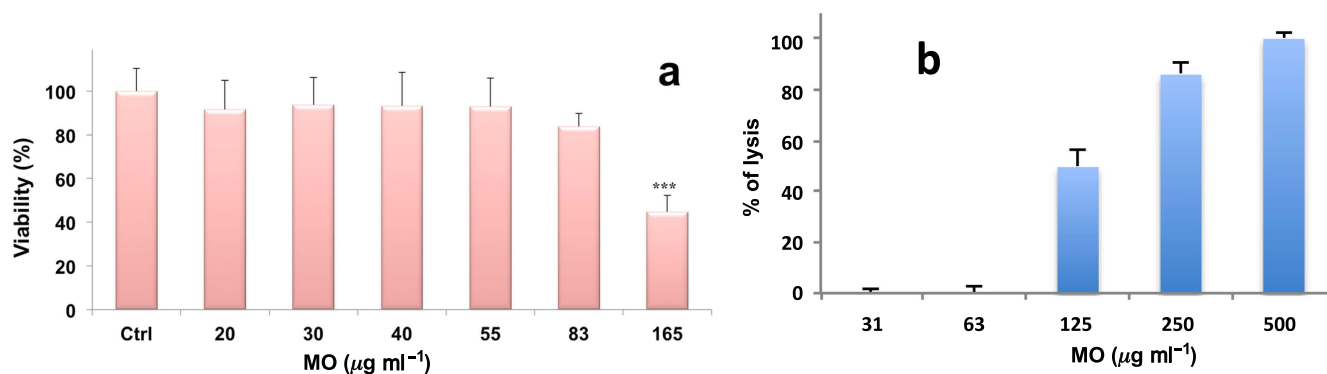


Figure 2. (a) Viability, expressed as % of the control, induced by incubation for 4 h with different concentrations of cubosomes (corresponding to 20–165 $\mu\text{g ml}^{-1}$ of MO) in 3T3 fibroblasts by MTT assay. Data are expressed as a mean \pm standard deviation (SD) of three independent experiments involving quadruplicate analyses for each sample; *** = $p < 0.001$ versus control. (b) Hemolysis test of human red blood cells incubated with different amounts of cubosomes in a standard hemolytic assay using 10% erythrocytes. Data were expressed as % of lysis \pm SD.

lipid-PEG conjugates may reduce their cytotoxicity [23, 45]. Accordingly, the proposed formulation was investigated for its cytotoxicity against 3T3 cells and erythrocytes. Several experiments reported in the literature evidenced that the cytotoxicity of cubosomes strongly depends on the cellular line investigated. However, the minimum dose reported of MO-based cubosomes necessary to induce cytotoxicity is around 20 $\mu\text{g ml}^{-1}$ of MO [10, 46–48]. The formulation here tested was found to induce no cytotoxicity in 3T3 cells up to 55 $\mu\text{g ml}^{-1}$ of MO (figure 2(a)).

Modifying a standard hemolytic assay [49] and using 10^9 erythrocytes (figure 2(b)) [50, 51], incubation of Cy5.5-C₁₄@cubosomes with human red blood cells evidenced the capacity of inducing direct lysis of erythrocytes in a dose-dependent manner. These results are in line with experiments previously reported [48, 52], and evidenced that our proposed cubosomes formulation did not provoke lysis of erythrocytes below 62 $\mu\text{g ml}^{-1}$ of MO.

Consequently, *in vivo* experiments were performed using a MO concentration of about 50 μg per ml of plasma. After *in vivo* injection of Cy5.5-C₁₄@cubosomes into the tail vein (i.v.) of a healthy mouse, distribution of the fluorophore was monitored using TD-OI. This technology was useful in understanding the lifetime distribution, and provided a convenient route of analyzing the biodistribution and plasmatic elimination of a fluorescent cubosomes formulation after i.v. administration in mice. Optical imaging was performed twice during the first day, then every 24 h for the next two days. Results showed that, following injection, Cy5.5-C₁₄@cubosomes were rapidly taken up by the liver (figure 3(a)).

To further investigate the extent of Cy5.5-C₁₄@cubosomes and/or free dye accumulation in organs and tissues, mice were sacrificed 48 h after injection of cubosomes for *ex vivo* TD-OI analysis of explanted organs (i.e., kidneys, thymus, heart, spleen, brain, lungs, stomach, intestine, and liver). This approach excludes any potential influence due to autofluorescence and scattering within the body and fur, thereby increasing both specificity and sensitivity of the probe detection. *Ex vivo* evaluation of organs 48 h post-injection

showed that the highest fluorescence intensity was localized in the liver and stomach, emphasizing that Cy5.5-C₁₄ is excreted through these organs (figure 3(b)).

Fluorescence lifetime information is complementary to intensity measurement and can be used to improve signal-to-background contrast and provide environment-sensing capability. Some biological events not available from fluorescent intensity images can be monitored directly from the fluorescence lifetime map. Fluorescence decays of Cy5.5-C₁₄@cubosomes and Cy5.5-C₁₄ were measured *in vitro*, and single-exponential models were appropriately fitted. Cy5.5-C₁₄ clearly changed its fluorescence lifetime properties once loaded in the cubosomes formulation (figure 3(c)).

This provided the possibility to discriminate *in vivo* between the Cy5.5-C₁₄@cubosomes and the free dye based on distinct lifetime profiles. Whole body imaging analysis a few minutes after i.v. injection revealed a diffuse distribution of cubosomes throughout the body of the mouse and, after the first 6 h, a strong signal decreasing over time and associated with the free dye, was clearly detectable mainly in the liver and intestine (figure 3(d)).

Cy5.5-C₁₄@cubosome plasmatic elimination after single i.v. administration was investigated by analyzing the fluorescence signal of plasma samples at different times post-injection. An exponential time decay of the average intensity suggested an underlying first-order kinetic (figure S4). Circulating profiles of the nanoparticles obtained from these experiments evidenced a half-life of approximately 2 h. This result is in good agreement with that reported on similar MO-based nanoparticles radiolabeled with a tracer molecule [12].

To cross-validate the results obtained *in vivo* and *ex vivo*, localization of Cy5.5-C₁₄ within the liver was confirmed by fluorescence microscopy examination of tissue cryo-sections obtained from the explanted organ 48 h after Cy5.5-C₁₄@cubosomes injection (figure 4). Close examination of the liver cryo-sections revealed the presence of several spherical fluorescent aggregates (indicated by the arrows) with size in the micrometer range, which could reasonably be identified as lipid droplets (cytoplasmic organelles involved in neutral lipid storage). Here, it is worth noticing that MO-

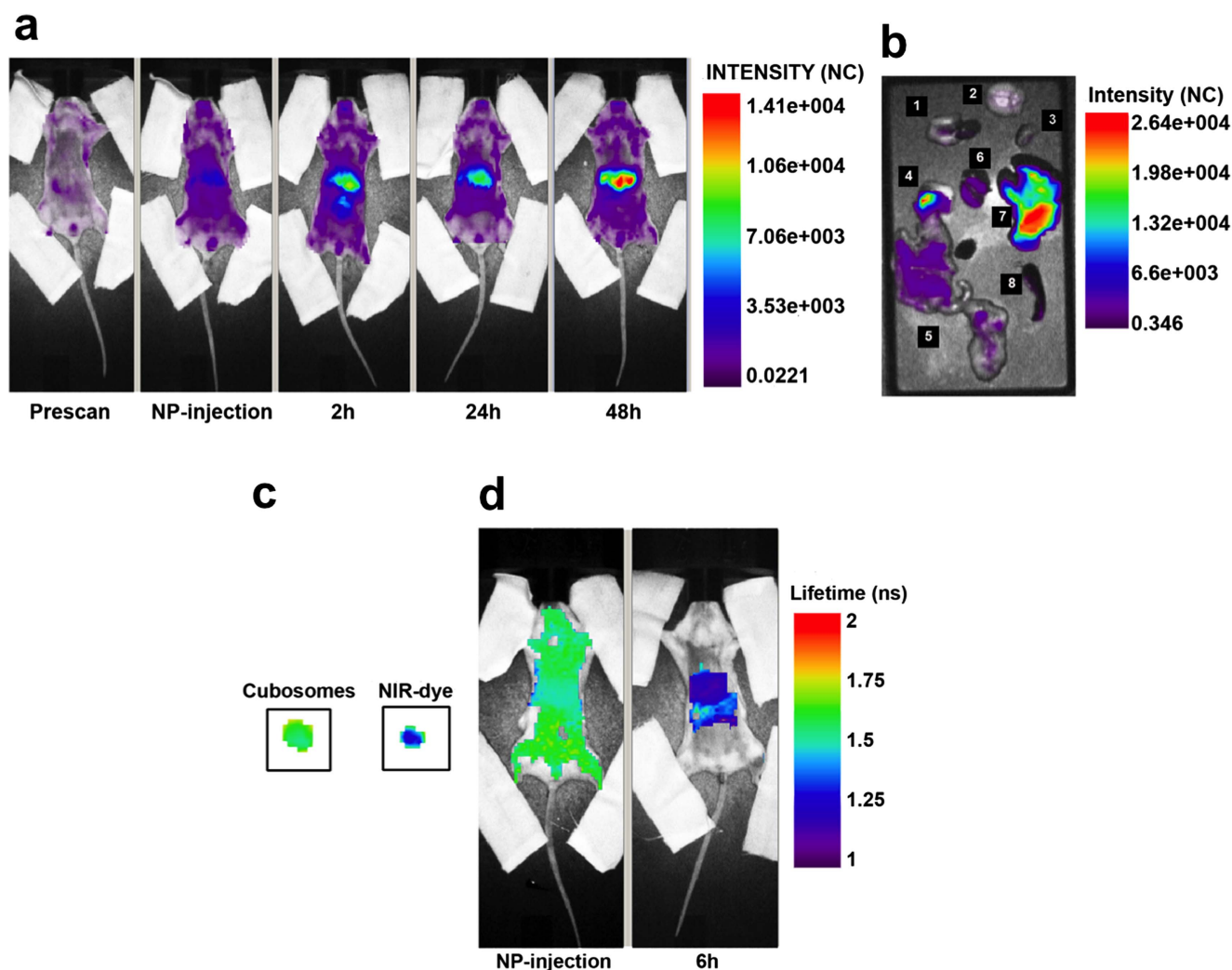


Figure 3. (a) Whole body fluorescence intensity distribution of a representative healthy mouse that received an i.v. injection of cubosomes ($150 \mu\text{l}$, corresponding to $\sim 0.4 \text{ nmol Cy5.5-C}_{14}$ and $50 \mu\text{g MO}$), displayed in NCs. Following injection, cubosomes were rapidly taken up by the liver. (b) In accordance to *in vivo* results, *ex vivo* analysis clearly showed that the highest signal of fluorescence emission was associated with the liver. 1. Lungs and heart; 2. Brain; 3. Thymus; 4. Stomach; 5. Intestine; 6. Kidney; 7. Liver; 8. Spleen. (c) *In vitro* fluorescence lifetime analysis with equimolar aliquots of the cubosome formulation and the control NIR-dye. Samples were placed on a paper substrate before lifetime analysis. Fluorescence lifetime maps were created from temporal point-spread function data acquired using the TD-FOI imaging system. (d) Representative *in vivo* fluorescence lifetime maps of whole body mice injected with cubosomes. Images were taken a few minutes and 6 h after the injection.

based nanoparticles (cubosomes, or vesicles) are readily internalized after exposure to cells, causing growth in the size and number of lipid droplets [21, 46, 53]. Moreover, given the high hydrophobic nature of Cy5.5-C_{14} , following nanoparticle disassembly after cellular internalization, the released dye should preferentially stain structures of this kind in the cells.

4. Conclusions

Cubosomes belong to a special class of nanoparticles characterized by the liquid crystalline nature of their nanostructure, and numerous recently published papers demonstrated their potential as diagnostic/theranostic tools. Here, an innovative cubosomes formulation loaded with an

NIR-emitting imaging dye to confer that these nanoparticles' fluorescent properties are useful for *in vivo* TD-FOI applications was investigated. Physicochemical analysis performed by SAXS confirmed the reverse cubic bicontinuous structure of the nanoparticles, and photophysical analysis proved that the fluorescence profile of the dye is retained after its encapsulation within the cubosomes, with a substantial increase in fluorescence lifetime. After intravenous administration at a non-cytotoxic concentration, TD-FOI analysis evidenced the diffuse distribution of the cubosomes throughout the whole body of the mouse and their intestinal and hepatic elimination with a first-order kinetic. Finally, we showed that the lifetime contrast could be used to distinguish cubosome fluorescence from free dye fluorescence and from nonspecific background signals.

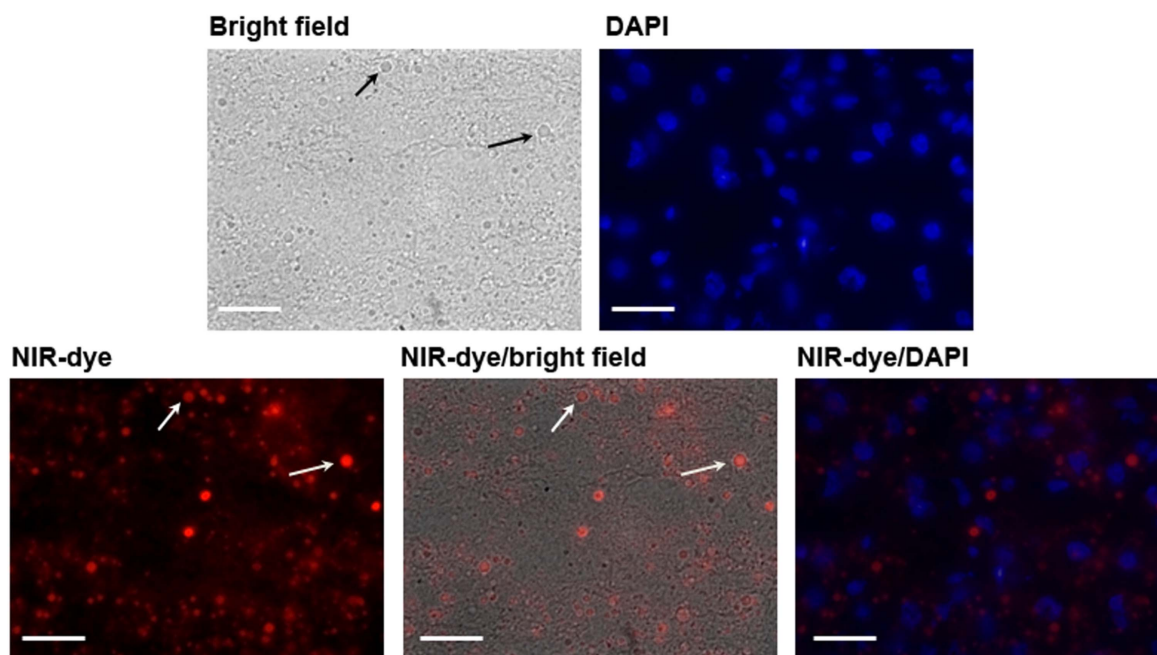


Figure 4. Representative microscopy images of cryo-sections obtained from liver explanted from the cubosomes-injected mice. Sections are imaged under bright field and fluorescence mode under x63. DAPI staining was conducted to visualize cell nuclei, which appear in blue, while Cy5.5-C₁₄ appears in red. The arrows indicate droplet structures in the hepatic parenchyma (bar = 15 μ m).

Because of its high sensitivity, FOI has been increasingly applied in assessing tissue pathology, such as in image-guided surgery, and for sentinel lymph node fluorescence mapping. In this respect, several intraoperative NIR fluorescence systems are now available for preclinical and clinical studies, and some have been approved by the FDA for use in humans [54]. In addition, fluorescence lifetime imaging is a powerful tool in investigating the molecule microenvironment, and has been widely used in modern microscopy. A combination of environmental sensitivity and chemical properties renders fluorescence lifetime as a separate yet complementary approach to conventional fluorescence intensity analysis. However, despite its significant impact in the context of microscopy, fluorescence lifetime imaging *in vivo* for applications in medical research has been delayed until the availability of a commercial time-domain imager.

From a molecular imaging perspective, it was here noted that cubosomes have great application potential in medicine as fluorescence and lifetime probes. For this purpose, more progress of fluorescent cubosomes toward *in vivo* applications will depend on the introduction of targeting properties that will increase the specificity of the cubosomes to be used for both imaging and therapeutic applications.

Acknowledgments

Fondazione Banco di Sardegna and Regione Autonoma della Sardegna (CRP-59699) are gratefully acknowledged. The cryo-TEM work was performed at the Technion Laboratory for Electron Microscopy of Soft Matter, supported by the Technion Russell Berrie Nanotechnology Institute (RBNI).

References

- [1] Hyde S T 1996 Bicontinuous structures in lyotropic liquid crystals and crystalline hyperbolic surfaces *Curr. Opin. Solid State Mater. Sci.* **1** 653–62
- [2] Hyde S, Ninham B W, Andersson S, Larsson K, Landh T, Blum Z and Lidin S 1997 *The Language of Shape* (Amsterdam: Elsevier)
- [3] Larsson K 1983 Two cubic phases in monoolein water system *Nature* **304** 664
- [4] Mulet X, Boyd B J and Drummond C J 2013 Advances in drug delivery and medical imaging using colloidal lyotropic liquid crystalline dispersions *J. Colloid Interface Sci.* **393** 1–20
- [5] Demurtas D, Guichard P, Martiel I, Mezzenga R, Hebert C and Sagalowicz L 2015 Direct visualization of dispersed lipid bicontinuous cubic phases by cryo-electron tomography *Nat. Commun.* **6** 8915
- [6] Gustafsson J, Ljusberg-wahren H and Almgren M 1996 Cubic lipid-water phase dispersed into submicron particles *Langmuir* **12** 4611–3
- [7] Landh T 1994 Phase behavior in the system pine oil monoglycerides-poloxamer 407-water at 20 °C *J. Phys. Chem.* **98** 8453–67
- [8] Azmi I D, Moghimi S M and Yagmur A 2015 Cubosomes and hexosomes as versatile platforms for drug delivery *Ther. Deliv.* **6** 1347–64
- [9] Meli V *et al* 2015 Docetaxel-loaded fluorescent liquid-crystalline nanoparticles for cancer theranostics *Langmuir* **31** 9566–75
- [10] Deshpande S, Venugopal E, Ramagiri S, Bellare J R, Kumaraswamy G and Singh N 2014 Enhancing cubosome functionality by coating with a single layer of poly- ϵ -lysine *ACS Appl. Mater. Interfaces* **6** 17126–33
- [11] Murgia S *et al* 2015 Cubosome formulations stabilized by a dansyl-conjugated block copolymer for possible nanomedicine applications *Colloids Surfaces B* **129** 87–94

- [12] Muir B W *et al* 2012 Metal-free and MRI visible theranostic lyotropic liquid crystal nitroxide-based nanoparticles *Biomaterials* **33** 2723–33
- [13] Boge L, Bysell H, Ringstad L, Wennman D, Umerska A, Cassisa V, Eriksson J, Joly-Guillou M-L, Edwards K and Andersson M 2016 Lipid-based liquid crystals as carriers for antimicrobial peptides: phase behavior and antimicrobial effect *Langmuir* **32** 4217–28
- [14] Kim H and Leal C 2015 Cuboplexes : topologically active siRNA delivery *ACS Nano* **9** 10214–26
- [15] Chong J Y T, Mulet X, Postma A, Keddie D J, Waddington L J, Boyd B J and Drummond C J 2014 Novel RAFT amphiphilic brush copolymer steric stabilisers for cubosomes: poly(octadecyl acrylate)-block-poly (polyethylene glycol methyl ether acrylate) *Soft Matter* **10** 6666–76
- [16] Chong J Y T, Mulet X, Waddington L J, Boyd B J and Drummond C J 2011 Steric stabilisation of self-assembled cubic lyotropic liquid crystalline nanoparticles: high throughput evaluation of triblock polyethylene oxide-polypropylene oxide-polyethylene oxide copolymers *Soft Matter* **7** 4768
- [17] Chong J Y T, Mulet X, Waddington L J, Boyd B J and Drummond C J 2012 High-throughput discovery of novel steric stabilizers for cubic lyotropic liquid crystal nanoparticle dispersions *Langmuir* **28** 9223–32
- [18] Johnsson M, Barauskas J, Norlin A and Tiberg F 2006 Physicochemical and drug delivery aspects of lipid-based liquid crystalline nanoparticles: a case study of intravenously administered propofol *J. Nanosci. Nanotechnol.* **6** 3017–24
- [19] Barreto J A, O'Malley W, Kubeil M, Graham B, Stephan H and Spiccia L 2011 Nanomaterials: applications in cancer imaging and therapy *Adv. Mater.* **23** H18–40
- [20] García K P, Zarschler K, Barbaro L, Barreto J A, O'Malley W, Spiccia L, Stephan H and Graham B 2014 Zwitterionic-coated 'stealth' nanoparticles for biomedical applications: recent advances in countering biomolecular corona formation and uptake by the mononuclear phagocyte system *Small* **10** 2516–29
- [21] Caltagirone C *et al* 2014 Cancer-cell-targeted theranostic cubosomes *Langmuir* **30** 6228–36
- [22] Zhai J *et al* 2015 Epidermal growth factor receptor-targeted lipid nanoparticles retain self-assembled nanostructures and provide high specificity *Nanoscale* **7** 2905–13
- [23] Jain V, Swarnakar N K, Mishra P R, Verma A, Kaul A, Mishra A K and Jain N K 2012 Paclitaxel loaded PEGylated glyceryl monooleate based nanoparticulate carriers in chemotherapy *Biomaterials* **33** 7206–20
- [24] Nilsson C *et al* 2013 SPECT/CT imaging of radiolabeled cubosomes and hexosomes for potential theranostic applications *Biomaterials* **34** 8491–503
- [25] Bye N, Hutt O E, Hinton T M, Acharya D P, Waddington L J, Mo B A, Wright D K, Wang H X, Mulet X and Muir B W 2014 Nitroxide-loaded hexosomes provide MRI contrast *in vivo* *Langmuir* **30** 8898–8906
- [26] Li X, Gao X, Shi W and Ma H 2014 Design strategies for water-soluble small molecular chromogenic and fluorogenic probes *Chem. Rev.* **114** 590–659
- [27] Luo S, Zhang E, Su Y, Cheng T and Shi C 2011 A review of NIR dyes in cancer targeting and imaging *Biomaterials* **32** 7127–38
- [28] Schätzel K 1991 Suppression of multiple scattering by photon cross-correlation techniques *J. Mod. Opt.* **38** 1849–65
- [29] Umezawa K, Citterio D and Suzuki K 2014 New trends in near-infrared fluorophores for bioimaging *Anal. Sci.* **30** 327–49
- [30] Gabbani T, Manetti N, Bonanomi A G, Annese A L and Annese V 2015 New endoscopic imaging techniques in surveillance of inflammatory bowel disease *World J. Gastrointest. Endosc.* **7** 230–6
- [31] Agostinis C *et al* 2011 *In vivo* distribution of β 2 glycoprotein I under various pathophysiological conditions *Blood* **118** 4231–8
- [32] Berenzin M Y, Lee H, Akers W, Guo K, Goiffon R J, Almutairi A, Fréchet J M and Achilefu S 2009 Engineering NIR dyes for fluorescent lifetime contrast *Conf. Proc. IEEE Eng. Med. Biol. Soc.* pp 114–7
- [33] Biffi S, Garrovo C, Macor P, Tripodo C, Zorzet S, Secco E, Tedesco F and Lorusso V 2008 *In vivo* biodistribution and lifetime analysis of Cy5.5-conjugated rituximab in mice bearing lymphoid tumor xenograft using time-domain near-infrared optical imaging *Mol. Imaging* **7** 272–82
- [34] Biffi S *et al* 2014 Multiple dye-doped NIR-emitting silica nanoparticles for both flow cytometry and *in vivo* imaging *RSC Adv.* **4** 18278
- [35] Garrovo C, Bergamin N, Bates D, Cesselli D, Beltrami A P, Lorenzon A, Ferrari R, Alberto Beltrami C, Lorusso V and Biffi S 2013 *In vivo* tracking of murine adipose tissue-derived multipotent adult stem cells and *ex vivo* cross-validation *Int. J. Mol. Imaging* **2013** 426961
- [36] Inagawa K, Oohashi T, Nishida K, Minaguchi J, Tsubakishita T, Yaykasli K O, Ohtsuka A, Ozaki T, Moriguchi T and Ninomiya Y 2009 Optical imaging of mouse articular cartilage using the glycosaminoglycans binding property of fluorescent-labeled octaarginine *Osteoarthr. Cartil.* **17** 1209–18
- [37] Rurack K and Spieles M 2011 Fluorescence quantum yields of a series of red and near-infrared dyes emitting at 600–1000 nm *Anal. Chem.* **83** 1232–42
- [38] Montalti M, Credi C, Prodi L and Gandolfi M T 2006 *Handbook of Photochemistry* (Boca Raton: CRC Press, Taylor and Francis Group)
- [39] Rosa A, Murgia S, Putzu D, Meli V and Falchi A M 2015 Monoolein-based cubosomes affect lipid profile in HeLa cells *Chem. Phys. Lipids* **191** 96–105
- [40] Marzari R, Sblattero D, Macor P, Fischetti F, Gennaro R, Marks J D, Bradbury A and Tedesco F 2002 The cleavage site of C5 from man and animals as a common target for neutralizing human monoclonal antibodies: *in vitro* and *in vivo* studies *Eur. J. Immunol.* **32** 2773–82
- [41] Abulrob A, Brunette E, Slinn J, Baumann E and Stanimirovic D 2007 *In vivo* time domain optical imaging of renal ischemia-reperfusion injury: discrimination based on fluorescence lifetime *Mol. Imaging* **6** 304–14
- [42] Angius R, Murgia S, Berti D, Baglioni P and Monduzzi M 2006 Molecular recognition and controlled release in drug delivery systems based on nanostructured lipid surfactants *J. Phys. Condens. Matter* **18** S2203–20
- [43] Barauskas J, Cervin C, Jankunec M, Špandryeva M, Ribokaitė K, Tiberg F and Johnsson M 2010 Interactions of lipid-based liquid crystalline nanoparticles with model and cell membranes *Int. J. Pharm.* **391** 284–91
- [44] Bode J C, Kuntsche J, Funari S S and Bunjes H 2013 Interaction of dispersed cubic phases with blood components *Int. J. Pharm.* **448** 87–95
- [45] Zhai J, Hinton T M, Waddington L J, Fong C, Tran N, Mulet X, Drummond C J and Muir B W 2015 Lipid-PEG conjugates sterically stabilize and reduce the toxicity of phantantriol-based lyotropic liquid crystalline nanoparticles *Langmuir* **31** 10871–80
- [46] Falchi A M, Rosa A, Atzeri A, Incani A, Lampis S, Meli V, Caltagirone C and Murgia S 2015 Effects of monoolein-based cubosome formulations on lipid droplets and mitochondria of HeLa cells *Toxicol. Res.* **4** 1025–36
- [47] Hartnett T E, Ladewig K, O'Connor A J, Hartley P G and McLean K M 2015 Physicochemical and cytotoxicity

- analysis of glycerol monoolein-based nanoparticles *RSC Adv.* **5** 26543–9
- [48] Tran N, Mulet X, Hawley A M, Hinton T M, Mudie S T, Muir B W, Giakoumatos E C, Waddington L J, Kirby N M and Drummond C J 2015 Nanostructure and cytotoxicity of self-assembled monoolein–capric acid lyotropic liquid crystalline nanoparticles *RSC Adv.* **5** 26785–95
- [49] Durigutto P, Macor P, Ziller F, De Maso L, Fischetti F, Marzari R, Sblattero D and Tedesco F 2013 Prevention of arthritis by locally synthesized recombinant antibody neutralizing complement component C5 *PLoS One* **8** e58696
- [50] Fridkis-Hareli M, Storek M, Mazsaroff I, Risitano A M, Lundberg A S, Horvath C J and Holers M V 2011 Design and development of TT30, a novel C3d-targeted C3/C5 convertase inhibitor for treatment of human complement alternative pathway-mediated diseases *Blood* **118** 4705–13
- [51] Zhang Y, Shao D, Ricklin D, Hilkin B M, Nester C M, Lambris J D and Smith R J H 2015 Compstatin analog Cp40 inhibits complement dysregulation *in vitro* in C3 glomerulopathy *Immunobiology* **220** 993–8
- [52] Hinton T M, Grusche F, Acharya D, Shukla R, Bansal V, Waddington L J, Monaghan P and Muir B W 2014 Bicontinuous cubic phase nanoparticle lipid chemistry affects toxicity in cultured cells *Toxicol. Res. (Camb)* **3** 11–22
- [53] Carboni M, Falchi A M, Lampis S, Sinico C, Manca M L, Schmidt J, Talmon Y, Murgi S and Monduzzi M 2013 Physicochemical, cytotoxic, and dermal release features of a novel cationic liposome nanocarrier *Adv. Healthcare Mater.* **2** 692–701
- [54] Mondal S B, Gao S, Zhu N, Liang R, Gruev V and Achilefu S 2014 Real-time fluorescence image-guided oncologic surgery *Adv. Cancer Res.* **124** 171–211